First total cross section measurements of ^{25,26}Mg(α, n) ^{28,29}Si via direct recoil detection

D. Blankstein, D. W. Bardayan, P. D. O'Malley, J. Allen, T. L. Bailey, C. Boomershine, E. Briley, D. P. Burdette, L. K. Callahan, S. Carmichael, A. M. Clark, A. C. Dombos, O. Olivas-Gomez, S. L. Henderson, L. Morales, A. D. Nelson, and J. Wilkinson

Department of Physics and Astronomy, University of Notre Dame, Notre Dame, Indiana 46556, USA

(Received 17 May 2024; revised 17 September 2024; accepted 1 October 2024; published 15 October 2024)

The ^{25,26}Mg(α, n) ^{28,29}Si reactions have been shown to be influential to ^{26}Al production in massive stars. The previously measured data sets for these reactions have discrepant results, and further study is warranted. The first measurements are reported of the total reaction cross sections of these reactions using direct recoil detection. The results are in good agreement with previous data sets based upon differential cross section studies. Astrophysical reaction rates based on the experimental data are reported and are within a factor of 1.5 of previous statistical model estimates.

DOI: 10.1103/PhysRevC.110.045803

I. INTRODUCTION

The definitive observations of ^{26}Al in our galaxy provided some of the first confirmations that nucleosynthesis is ongoing. The lifetime of ^{26}Al ($t_{1/2} = 7.2 \times 10^5$ yr), while long, is still much shorter than the estimated age of the Universe. A number of astrophysical environments may contribute to the galactic ^{26}Al abundance including asymptotic giant branch stars; massive and very massive stars, both their Wolf-Rayet winds and their final core-collapse supernovae (CCSN); and novae [1]. These are all sites that could synthesize ^{26}Al in hydrogen burning via the ^{25}Mg(p, γ) ^{26}Al reaction. However, the production rates predicted by models of these various sources contain large uncertainties, making it difficult to precisely account for their respective ^{26}Al contributions.

To better understand how ^{26}Al is produced in massive stars, it is necessary to have a good knowledge of the nuclear reactions taking place within them. Of particular importance is understanding the ^{25}Mg(α, n) ^{28}Si and ^{26}Mg(α, n) ^{29}Si reactions, which have been shown to strongly influence the final production of ^{26}Al in massive stars [2].

^{26}Al is produced in massive stars in three specific environments: core hydrogen burning, C/Ne convective shell burning, and explosive C/Ne shell burning [3]. ^{26}Al is produced in all of these environments via the ^{25}Mg(p, γ) ^{26}Al reaction and is destroyed primarily via β decay to ^{26}Mg. ^{25}Mg, which is a seed nucleus for ^{26}Al, is either present in the initial abundance of the star or is generated via the ^{24}Mg(p, γ) ^{25}Al(β^+) ^{25}Mg reaction.

^{26}Al is produced in hydrogen core burning once a star reaches main sequence burning. Typical core temperatures for this burning in massive stars are 40–90 MK [4]. After reaching a peak abundance 1–2 Myr after core hydrogen burning commences, the ^{26}Al abundance will continuously decline as β decay competes with production [3]. ^{26}Al produced in this hydrogen core burning can be ejected into the interstellar medium for very massive (mass greater than $30M_\odot$) stars classified as Wolf-Rayet stars. These stars experience a substantial mass loss from stellar winds that are strong enough that portions of the hydrogen core, where ^{26}Al was produced, are ejected out into the interstellar medium.

In C/Ne shells, ^{26}Al is produced in stable burning phases with temperatures of roughly 1.5 GK. In both of these shells ^{26}Al is again produced via ^{25}Mg(p, γ) ^{26}Al, with the higher temperatures increasing the rate of this reaction. In the carbon burning shell, seed ^{25}Mg is produced via the reaction ^{22}Ne(α, n) ^{25}Mg and protons are produced via the ^{12}C$(^{12}$C$, p)$ ^{23}Na and ^{23}Na(α, p) ^{26}Mg reactions. Convection in the carbon-burning shell is vital to the production of ^{26}Al because it brings newly synthesized ^{12}C and ^{25}Mg to the regions of efficient ^{26}Al production, and transports ^{26}Al to regions of lower temperature where its lifetime increases [3]. ^{26}Al is destroyed in this burning via neutron capture reactions with neutrons provided by the ^{22}Ne(α, n) ^{25}Mg and ^{12}C$(^{12}$C$, n)$ ^{23}Mg reactions.

Neon shell burning produces and destroys ^{26}Al in the same processes described for carbon shell burning. Protons are again generated from the ^{23}Na(α, p) ^{26}Mg reaction with α particles now supplied via ^{20}Ne photodisintegration. Again, convection plays an important role in the survival of ^{26}Al in this shell as the equilibrium abundance in a radiative environment will lead to a small ^{26}Al abundance due to its short lifetime at high temperatures.

In explosive C/Ne shell burning, following a core-collapse explosion, temperatures can briefly reach up to 2.3 GK. Production and destruction mechanisms are the same as described for stable shell burning; however, the ^{23}Na(α, p) ^{26}Mg reaction competes with the ^{23}Na(p, γ) ^{24}Mg reaction and ^{25}Mg(α, n) ^{28}Si competes with ^{25}Mg(p, γ) ^{26}Al [4]. ^{26}Al is again destroyed via neutron capture reactions.

A sensitivity study by Ilidias *et al.* [2] sought to determine which reaction rates and their uncertainties influenced the final abundance of ^{26}Al in the burning environments described above. This was accomplished by varying the

rates of different reactions by factors of 10, 2, 0.5, and 0.1 and analyzing which rates, when varied, had the largest impact on the ^{26}Al yield. To perform these calculations Iliadis and colleagues used the stellar models of Limongi and Chieffi [3].

For explosive Ne/C burning, this study found that one of the most influential rates, when varied, was the ^{25}Mg$(\alpha, n)^{28}$Si reaction rate. As mentioned above, this reaction destroys seed ^{25}Mg nuclei which would otherwise go on to produce ^{26}Al. For reasons that will be discussed in the next section, a reevaluation of the ^{25}Mg$(\alpha, n)^{28}$Si cross section and reaction rate are needed.

In convective C/Ne shell burning both the ^{25}Mg$(\alpha, n)^{28}$Si and ^{26}Mg$(\alpha, n)^{29}$Si reactions were found to impact the final abundance of ^{26}Al. These reactions produce neutrons that destroy ^{26}Al via neutron capture reactions. Similar arguments for reevaluating the ^{25}Mg(α, n) cross section and reaction rate apply to the ^{26}Mg(α, n) reaction and will be detailed in the next section.

The ^{26}Mg$(\alpha, n)^{29}$Si reaction also plays an important role in explosive C/Ne nucleosynthesis apart from the production of ^{26}Al. Isotopic abundances found in presolar grains allow us to compare and constrain models of stellar nucleosynthesis. Some grains have signatures of isotopes produced in CCSn with abundances of the decay products of radioactive nuclei including ^{26}Al. However, models of supernova nucleosynthesis fail to reproduce certain isotopic ratios found in these grains, such as the ^{29}Si/^{30}Si ratio.

The work of Hoppe *et al.* reported the discovery of a SiC grain (labeled KJB2-11-17-1) with an unusually strong enrichment of ^{29}Si and depletion of ^{30}Si [5]. In this work, it was suggested that the disparity in models and ratios found in grains can be attributed to the production of ^{29}Si. Hoppe *et al.* explored various reaction rates impacting final ^{29}Si abundances and found that the ^{26}Mg$(\alpha, n)^{29}$Si reaction played a crucial role in its synthesis in explosive C/Ne burning at temperatures and densities very similar to those for ^{26}Al production. They found that increasing the ^{26}Mg$(\alpha, n)^{29}$Si reaction rate by a factor of 1.8 reproduced the ^{29}Si/^{30}Si ratio found in the KJB2-11-17-1 SiC grain. It is clear an understanding of the reaction rate and cross section for this reaction is needed.

II. PREVIOUS STUDIES OF ^{25}Mg$(\alpha, n)^{28}$Si AND ^{26}Mg$(\alpha, n)^{29}$Si

The ^{25}Mg$(\alpha, n)^{28}$Si and ^{26}Mg$(\alpha, n)^{29}$Si cross sections have been studied; however, the experimental data exhibit discrepant results. All of the previous measurements outlined in this section, for both of these reactions, involve measurements solely in normal kinematics using a beam of α particles on a Mg target. The analyses of these measurements were often made difficult by the inability to characterize background reactions produced by contaminants in the target, by unmeasured neutron angular distributions resulting in uncertain estimates of the total cross sections, and by energy-dependent detection efficiencies that could change drastically if excited states were populated in the reactions. Such uncertainties have plagued other (α, n) cross section measurements (e.g., see Ref. [6]).

The first measurements were made in 1962 by Bair *et al.* with a study of the ^{26}Mg$(\alpha, n)^{29}$Si cross section [7]. The reaction was studied using an accelerated beam of α particles on MgO (99% ^{26}Mg) targets for α energies of 3.1–5 MeV. Neutrons were detected via a graphite-sphere neutron detector. The authors state they were unable to control or obtain the ratio of Mg to MgO in their targets. The presence of unknown contaminants in their targets led to large cross section uncertainties of 25–50%.

Measurements by Russell *et al.* [8] in 1972 studied the ^{26}Mg$(\alpha, n)^{29}$Si reaction down to 2.5 MeV using 99.7% enriched ^{26}Mg material evaporated onto thick Cu backings. Detection of neutrons was made via a BF_3 counter. Only spectroscopic information was obtained from this measurement, and total cross sections are not reported.

The ^{25}Mg$(\alpha, n)^{28}$Si reaction was first measured by Van der Zwan and Geiger in 1981 [9]. Measurements were made on Mg targets that were prepared by vacuum evaporation of ^{25}Mg (enriched to 98%) and by reduction of MgO with zirconium at high temperature, evaporating the metal. Target backings of silver, tantalum, and gold were used. Again, α particles were impinged on the Mg targets down to α energies of 2.0 MeV. Neutron yields were measured using stilbene crystals. The authors noted an error of 20 percent in their total cross section measurement.

Following the measurements of Van de Zwan and Geiger, Anderson *et al.* performed measurements of both the ^{25}Mg$(\alpha, n)^{28}$Si and ^{26}Mg$(\alpha, n)^{29}$Si cross sections in 1983 [10]. Anderson and colleagues were motivated by the work of Howard *et al.* [11], which posited that neutron-rich nuclei were produced in explosive environments with high neutron fluxes, such as explosive carbon burning. Anderson and colleagues sought to determine whether a major source of these neutrons could be the ^{25,26}Mg$(\alpha, n)^{28,29}$Si reactions in explosive neon burning. These reactions were studied using an α beam on Mg targets with α energies of 1.8 to 6.0 MeV for ^{25}Mg (97.9% enriched) and 2.1 to 6.0 MeV for ^{26}Mg (99.7% enriched). Evaporated targets of MgO on tantalum backings were used. Detection methods included BF_3 tubes embedded in paraffin to measure the neutrons, and a germanium detector to measure gamma rays from the excited Si nucleus. Neutron detector efficiencies for detectors of this type are energy dependent, and Anderson *et al.* performed direct measurements of their detection efficiency. Statistical-model calculations were used to determine the branching ratios of gamma rays emitted from the Si-excited states. This allowed for simultaneous cross sections measurements from the neutron yields as well as gamma ray measurements. Total cross sections reported from both detection methods were in good agreement. Below roughly 2.0 MeV, significant contributions from background reactions were observed in the neutron yields. Below this energy, the cross sections from the neutron detector data are therefore reported as upper limits.

The most recent measurement of ^{25}Mg$(\alpha, n)^{28}$Si was made by Caciolli *et al.* in 2014 [12]. α particles with energies from 3 to 5 MeV were impinged on a target of MgO (95.8% enriched ^{25}Mg) evaporated on gold. Target contamination was analyzed

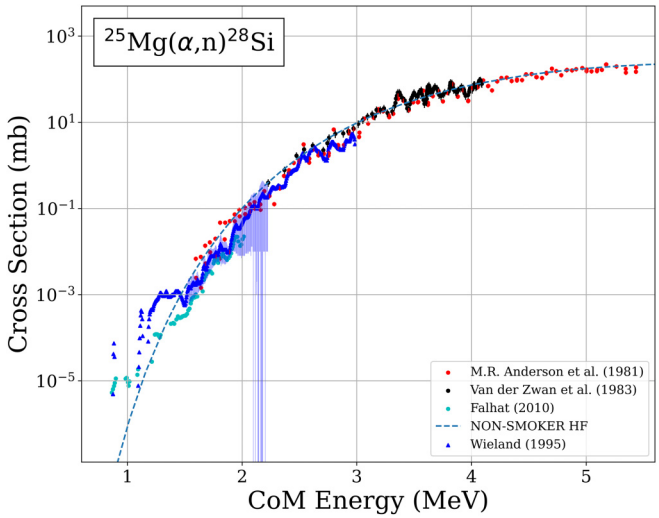

FIG. 1. Previous measurements of the ^{25}Mg$(\alpha, n)^{28}$Si total cross section. Anderson and Van der Zwan data consist of published cross section data whereas the Wieland and Falahat data are from unpublished dissertations.

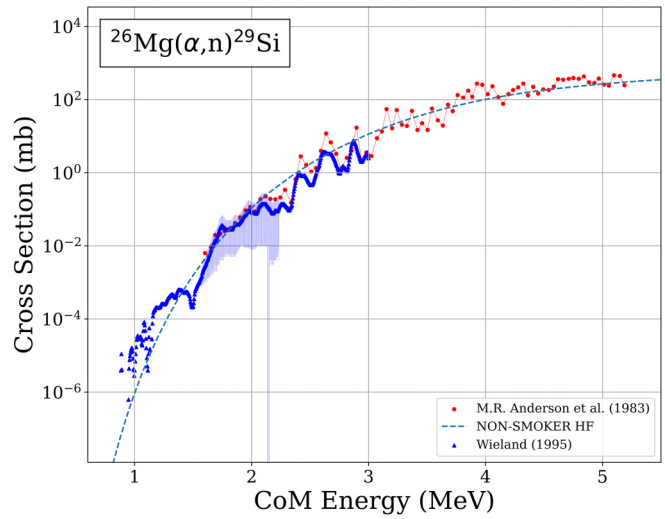

FIG. 2. Previous measurements of the ^{26}Mg$(\alpha, n)^{29}$Si total cross section. The Anderson data represent published data whereas the Wieland data are from unpublished thesis work.

via Rutherford backscattering spectroscopy. Detailed angular distributions of neutrons were measured via an array of liquid scintillator detectors from angles of 17.5 to 106 degrees. The authors note that, from their measurements, more detailed angular information is needed in order to extract total integrated cross sections, and they did not report any total cross section data.

Apart from the published data, the ^{25,26}Mg$(\alpha, n)^{28,29}$Si reaction has been the subject of Ph.D. dissertations. One such work is that of Wieland in 1995 [13] which measured these reactions to gauge their astrophysical impact as neutron sources, similar to the motivation of Anderson *et al.* [10]. Measurements were made using a 4π neutron detection setup consisting of 16 ^{3}He tubes embedded in an polyethylene matrix. This setup allowed for the highly efficient measurement of neutrons. However, a neutron detector of this type requires knowledge of the detector efficiency as a function of energy, and Wieland did not report any detailed information on their detector efficiency. Wieland used implanted targets to avoid background due to impurities. Gold-plated copper backings were used for the targets. The observation of ^{13}C$(\alpha, n)^{16}$O (presumably from hydrocarbon contamination) from the target meant that background contamination made it difficult to extract neutron yields from the Mg reactions.

Measurements of these reactions were also made in the Ph.D. work of Falahat in 2010 [14]. This work, following the same motivation as the Wieland work, sought to measure both the ^{25,26}Mg$(\alpha, n)^{28,29}$Si cross sections in the energy range from 2.7 down to 0.7 MeV α energies. As with previous measurements, impurities in the target (98.8% enriched but with other chemical impurities) introduced a significant background. After performing substantial corrections due to this background, they reported cross section measurements for both reactions that were lower than previous measurements.

The combined measured cross section data for both of these reactions are shown in Figs. 1 and 2. The data from Anderson *et al.* represents the extracted cross section from the neutron detector measurement as well as the gamma ray measurements. For the ^{25}Mg$(\alpha, n)^{28}$Si reaction, in the center-of-mass energy region above 3.0 MeV, the Anderson and Van der Zwan data show good agreement between data sets. Below this energy range, there are some discrepancies between all the data sets. The Wieland data are consistently lower than the Anderson data in this energy range below 3.0 MeV. Below 2.0 MeV the Anderson data are considered upper limits. Below 1.5 MeV the Wieland data are upper limits. Work is needed to resolve discrepancies in the cross section data at low energy. It is also important to perform measurements using complementary techniques with different systematics. With respect to the previous measurements, it is important to use a different technique utilizing a target without spectator atoms.

For the ^{26}Mg$(\alpha, n)^{29}$Si reaction, a similar situation exists between the Wieland data and Anderson data, with the Wieland data consistently lower than the Anderson data. At energies below 2.2 MeV the Anderson data are upper limits only, and below 1.5 MeV the Wieland data are only considered upper limits. It is clear that more data are needed throughout the previously measured energy range to confirm the measurements at higher energies and resolve discrepancies in the data at lower energies.

III. MEASUREMENT OF THE ^{25,26}Mg$(\alpha, n)^{28,29}$Si TOTAL CROSS SECTIONS

Measurements of the ^{25,26}Mg$(\alpha, n)^{28,29}$Si cross sections were made at The University of Notre Dame's Nuclear Science Lab using the Active Target High Efficiency detector for Nuclear Astrophysics (ATHENA) [15]. ATHENA utilizes an active target approach to efficiently measure total cross sections. A discussion of the construction and commissioning,

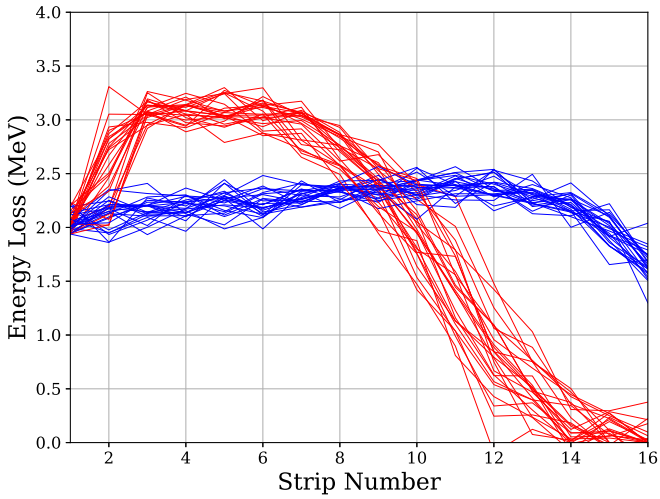

FIG. 3. Simulated beam and (α, n) reaction events occurring in strip 2 for the 350 Torr ^{26}Mg experimental run. Reaction locations in strip 2 and emission angles are randomly sampled to generate the traces in this plot.

along with the details of the operating principle of ATHENA can be found in [15].

Measurements with ATHENA offer a complementary approach to the measurements outlined in the previous section. ATHENA utilizes a method in which the heavy Si recoils are detected instead of the reaction neutrons, resulting in measurements of total cross sections that are independent of neutron angular distributions, neutron detection efficiencies, and the population of excited states in the residual nuclei. The measurements are also self-normalizing since both the beam and residual reaction nuclei are detected. The measurements are much less sensitive to contaminants since the incident ^{25,26}Mg beams are mass analyzed before impinging on the pure He target.

A drawback of this method is that the resolution expected in the excitation function will be somewhat worse than the normal-kinematics measurements, so the extracted data should be viewed as a check on the overall scale of the cross sections rather than a measure of the excitation function fine structure. Also, since the active target/detector must detect both the beam and the recoils, incident beam currents must be limited to prevent pileup and data acquisition dead time resulting in a reduced ability to measure very small cross sections. A simulation of the expected trace plots for the beam and (α, n) reactions is shown in Fig. 3. The events of interest should be clearly separable by virtue of their easily distinguishable energy loss pattern.

Beams of ^{25}Mg and ^{26}Mg were produced by a multicathode source of negative ions via cesium sputtering (MC-SNICS). ^{25}Mg and ^{26}Mg comprise 10.00% and 11.01% of natural Mg, respectively. Cathodes were filled with a compacted mixture of Mg powder and Titanium hydride powder (Mg+TiH_2) which resulted in $^{25,26}MgH^-$ ions from the source. Typical Mg beam rates produced from MC-SNICS were 1 and 2 nA for ^{25}Mg and ^{26}Mg, respectively. While these were relatively low rates compared to that of a beam such as ^{12}C, they were more than enough to reach the 4 kHz maximum usable rate of ATHENA before dead time becomes prohibitive. Due to the low beam production rate, a ^{24}Mg beam was tuned through the accelerator to ATHENA first and then the beam was switched to ^{25,26}Mg. This allowed tuning through the accelerator and various elements with enough primary beam to optimize on various Faraday cups. Once the optimal tune was found with ^{24}Mg, the beam was then switched to either ^{25}Mg or ^{26}Mg, and final adjustments were made to optimize those beams.

TABLE I. The beams, He gas pressures, and energies used in the ^{25,26}Mg$(\alpha, n)^{28,29}$Si measurements.

Beam	Pressure (Torr)	Beam energy (MeV)	$\Delta E_{\text{c.m.}}$ (MeV)
^{25}Mg	225	50	4.6 – 3.5
^{25}Mg	275	47	3.9 – 3.2
^{26}Mg	300	50	5.0 – 3.1
^{26}Mg	350	56	4.1 – 3.0

After each of the Mg beams were produced, they were transported through the low-energy ∼1/200 mass resolution injection system [16] and accelerated by the FN tandem pelletron accelerator. During the acceleration stage, the $^{25,26}MgH^-$ ions are broken up by the carbon stripper foil, and electrons are stripped from the ^{25,26}Mg ion which results in positive ions for the second stage of tandem acceleration. This resulted in pure ^{25,26}Mg beams after the acceleration stage. The beam was then focused and transported to the detector via steering and focusing elements. Along the beam path, a pair of 1/2000 attenuators were used to reduce the beam rate down to a rate that ATHENA could handle. Due to the low primary beam rate, only one of the attenuators was used. A collimator placed approximately 10 cm upstream of ATHENA was used to reduce scattered beam and produced a 1-cm-diameter beam spot on the 6.15-μm-thick 2.8-cm-diameter Mylar entrance window.

The total cross section measurement utilized a variety of different beam energies and gas pressures within ATHENA. The Gamow window for ^{25}Mg$(\alpha, n)^{28}$Si at $T = 2.3$ GK, a temperature relevant for explosive Ne/C burning, is 1.8–3.5 MeV in the center-of-mass energy frame. The Gamow window for ^{26}Mg$(\alpha, n)^{29}$Si, again at temperatures relevant for explosive Ne/C burning, is 1.8–3.5 MeV in the center-of-mass energy frame. A high-energy measurement and low-energy measurement were made for each Mg isotope. The goal of using different pressures/energies was to make independent measurements that probe the cross section with overlapping energies. Consistency between the measured cross sections helps ensure the validity of the measurements. A table showing the different beam energies and pressures used for both beams is shown in Table I. With these measurements, we measured above and into the Gamow window for explosive Ne/C burning for both of these reactions.

One important aspect of measuring the (α, n) reactions for ^{25,26}Mg is the potential presence of (α, p) reactions. The Q values for (α, n) and (α, p) for both Mg beams are shown in Table II. The energy region of interest in ATHENA for each configuration is above the threshold for the (α, p) reaction. As

TABLE II. Reaction Q values.

Reaction	Q value (MeV)
^{25}Mg$(\alpha, n)^{28}$Si	2.653
^{25}Mg$(\alpha, p)^{28}$Al	−1.206
^{26}Mg$(\alpha, n)^{29}$Si	0.034
^{26}Mg$(\alpha, p)^{29}$Al	−2.871

a result, some (α, p) events may be observed; however, a lack of previous cross section data in the relevant energy range for the (α, p) reactions made it difficult to estimate to what extent they would be present in measurements. Simulations similar to the one shown in Fig. 3 show that, given the resolution of ATHENA if the (α, p) reactions are present, they will be separable from the (α, n) reactions.

IV. ANALYSIS

A. Event filtering

A trace plot of the data acquired from the ^{26}Mg 350 Torr measurement is shown in Fig. 4. Apparent in Figure 4 is the most intense feature, the beam. Extending in energy above the beam are pileup events. Also embedded in the region above the beam are potential events from reactions occurring in the gas.

To identify these reaction events, an event-filtering process is employed to separate out background events, leaving only events resulting from the (α, n) and potentially (α, p) reactions. Beamlike events are considered events that have an energy loss within ±150 keV (the rough energy loss spread observed) of the mean energy in each strip. In strip 1, all events are gated on having a beamlike energy. This eliminates pileup events, and any reaction or scattering events occurring in the dead space before the first strip or in the window. Some scattering events will inevitably make it through this step if they have an energy loss very close to that of the beam in strip 1.

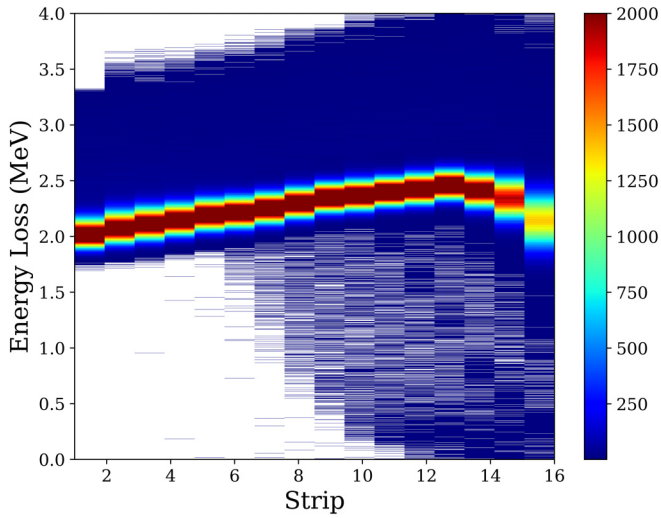

FIG. 4. Trace plot of data before event filtering from the 350 Torr ^{26}Mg run.

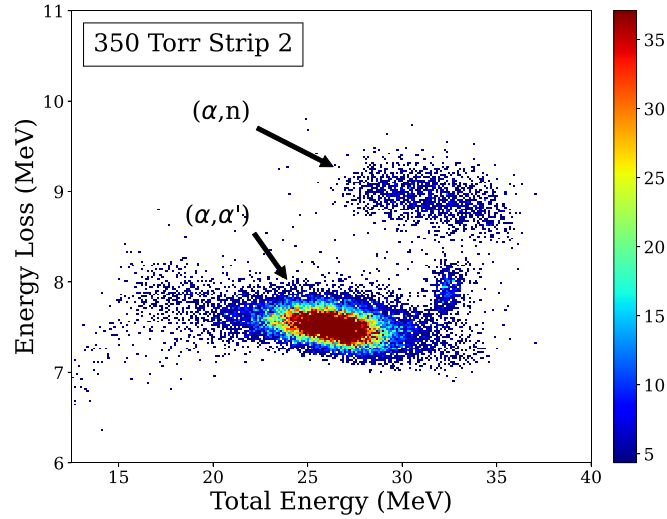

FIG. 5. Summed energy loss in strips 3, 4, and 5 vs total energy deposited in ATHENA. Events shown are those remaining after event-filtering steps 1–5 for reactions occurring in strip 2.

To determine events occurring from reactions in a given strip, a condition is placed that, in all strips before that strip, energy losses are beamlike only. This eliminates events from reactions occurring before that strip and ensures that only beamlike events occur before. A gate is then placed on the energy loss of the events to accept only events with an energy loss higher than that of the beam in that strip and the following one since reactions produce a sudden jump in energy loss due to the heavier recoil (in this case ^{28,29}Si) having a higher Z than that of the beam. The reason for also including the following strip is to eliminate possible gas scattering events and to ensure that random fluctuations are not included in the pool of reaction events. Only two strips are used because the trace of the reaction product tends to decrease quickly after the reaction occurs (see Fig. 3).

In order to reduce background scattering events, an additional condition is placed to accept only events that have an energy loss lower than that of the beam by strip 16, the last active strip. Some of the background scattering events will have an energy loss very similar to that of the beam by strip 16. However, due to the higher Z of the reaction products from (α, n), the energy loss of those events will be much lower in energy loss than that of the beam by the time they reach the 16th strip (see Fig. 3).

In Fig. 5, an energy loss plot analyzing reactions in strip 2 from the ^{26}Mg 350 Torr measurement is shown. The energy loss on the y axis is generated by the sum of energy loss in strips 3, 4, and 5. The reason for choosing strips 3, 4, and 5 instead of 2, 3, and 4 when analyzing reactions occurring in strip 2 is the following: the energy loss in strip 2 will exhibit a wide variation in energy for the reaction products. This occurs because there are a range of locations in strip 2 where reactions can take place. For example, for a reaction occurring at the very beginning of strip 2, the energy loss will be high since, for the majority of the path along strip 2, the particle has

higher charge and deposits greater energy. In the case where the reaction occurs at the end of the strip, the energy loss is much closer to that of the beam. Thus, it is observed in the (α, n) traces that, in the strip where the reaction occurs, a wide variation is observed. In the strips after the reaction strip, a much more consistent energy loss is observed. By plotting the energy loss in strips 3, 4, and 5 for reactions occurring in strip 2, we achieve a clearer separation of reaction events.

In Fig. 5, multiple features are observed. Labeled (α, α') are events that are either scattering off of the helium gas or the detector window. These events exhibit an energy loss higher than that of the beam hence they can make it through the filtering process of the first five steps. At higher energy loss is a clear group of (α, n) events. These events are well separated from the other groups in this plot. One more feature of this plot, unique to the ^{26}Mg measurements, is the presence of a faint beam contaminant. At approximately 32 MeV in total energy, and above the (α, α') scattering events, is a faint group of events showing a contaminant in the beam itself. These events had a much more narrow energy spread, indicating that they were in the primary beam and not the result of a reaction. In order to ensure these events were from a contaminant in the beam, and not arising from reactions in the gas, the target gas in ATHENA was replaced with P10 (10% argon and 90% methane) gas, and the same contaminant feature was observed with the same intensity when measured with helium gas. This confirms that this contaminant is in the beam itself, and not arising from reactions occurring in the detector. This beam contaminant was not observed in the ^{25}Mg measurements. Based on Fig. 5 showing an energy loss intermediate to the $Z = 12$ and $Z = 14$ groups and the fact that the contaminant is not observed in the ^{25}Mg runs, one can surmise that the weak contaminant is most likely ^{27}Al that was injected along with the ^{26}MgH molecule into the FN tandem. The contaminant did not interfere with the (α, n) region of interest in Fig. 5 and was therefore not a problem for the analysis.

Finally, in order to better separate events and probe the presence of (α, p) events, energy-loss-averaged plots are analyzed. To produce these plots, an N and $N + 1$ strip average is taken from the peak of the energy loss trace, where N is the number of strips for which the energy loss is averaged. The N-strip average is plotted on the x axis, and the $N + 1$-strip average is plotted on the y axis. This process was first used in the analysis of data from the MUSIC detector by Avila *et al.* to separate (α, n) and (α, p) events [17]. As seen in Fig. 6, different event types are clearly separated and labeled. The separation of events in Fig. 6 indicates events from the (α, p) reaction may be present in the measurement; however, with the beam contaminant, it is difficult to confidently ascribe these events arising from (α, p) reactions. Regardless, it is clear that they are well separated from (α, n) events and do not effect extraction of their yield.

B. Beam energy losses

In addition to identifying events of interest, another important consideration was determining the energies at which a given reaction occurs. Understanding the beam energy losses as it traverses the window and gas at different pressures was important to determine the center of mass energies at which the cross sections were being measured. To address these uncertainties, a silicon surface-barrier detector was installed on the downstream end of ATHENA and calibrated by impinging a low-intensity ^{25,26}Mg beam directly on it without the ATHENA window and target gas. Once calibrated, the window was inserted into the beam line, and the energy loss directly measured. This was performed at several bombarding energies between 45–60 MeV. Afterward He gas was introduced into ATHENA at various pressures, and the energy loss of the beam was measured again. Since it was not possible to measure the energy at every single strip, the goal was to compare energy loss measurements with model predictions that would then be used to estimate the reaction energies as a function of strip number. The results of the measurements are compared with predictions from TRIM [18], LISE++ [19], and STOPIT [20] in Fig. 7. The closest predictions were found to be with the STOPIT code, and thus it was used during subsequent analysis.

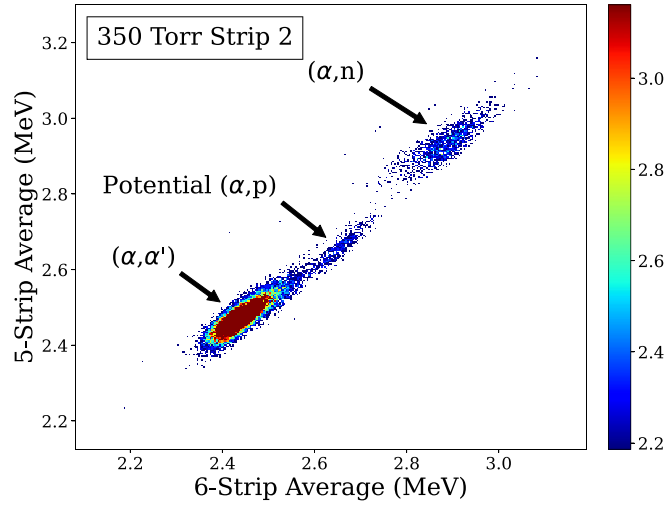

FIG. 6. Five-strip vs six-strip averaged correlated energy loss plot from strip 2 from the 350 Torr ^{26}Mg run. Clear separation between (α, n), potential (α, p), and (α, α') events is observed.

V. RESULTS

Since the cross sections drop at lower energies (i.e., later strips in ATHENA), there was always a threshold strip after which too few events were observed to extract a cross section. Each configuration of pressure and energy typically resulted in 4–8 strips with high enough yields to extract cross sections. The extracted cross sections from these measurements are shown in Figs. 8 and 9 along with the previously published data in this energy range. The uncertainties in ATHENA cross section data are statistical. The error bars in the energy measurement represent the inherent ambiguity in where reactions occur within the reaction strip. Therefore, the error bar represents the center-of-mass energy loss which covers the entire strip and is much larger than the 10% uncertainties found for the predicted energy losses per strip. The cross section value

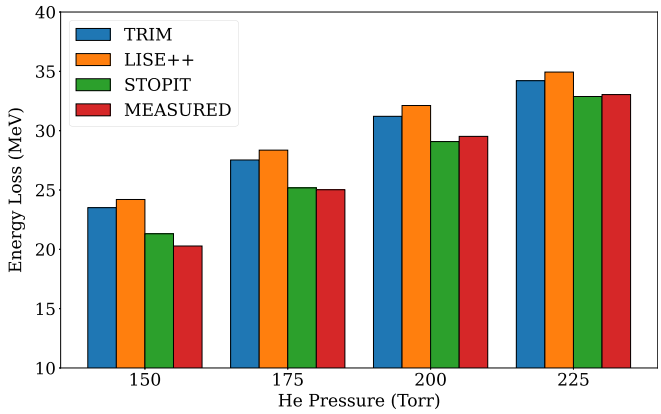

FIG. 7. The energy loss of Mg beams was measured as a function of gas pressure in ATHENA. A comparison is made to various energy loss predictions, with the calculations by STOPIT [20] being the closest. On average the predictions were within 10% of the measured energy losses.

is assigned to the center-of-mass energy of the beam at the geometric center of the strip.

The cross section measurements from ATHENA, for both reactions, show good agreement with the previously measured data by Anderson *et al.* and Van der Zwan *et al.* indicating that the previous measurements properly accounted for neutron angular distributions and efficiencies in their analyses.

VI. ^{25,26}Mg$(\alpha, n)^{28,29}$Si REACTION RATE CALCULATIONS

The cross section measurements described in the previous section provide confirmation to previous measurements of the ^{25,26}Mg$(\alpha, n)^{28,29}$Si total cross section. By measuring the reaction in inverse kinematics, using a beam of ^{25,26}Mg on a target of high-purity helium, an entirely different method for extracting the total cross section is utilized. The cross section data from ATHENA shows good agreement with the

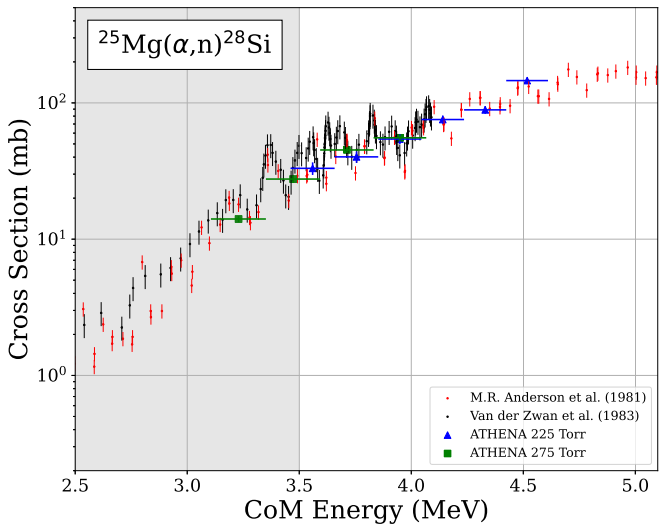

FIG. 8. Extracted total cross section for ^{25}Mg$(\alpha, n)^{28}$Si. The shaded area indicates the Gamow window for C/Ne burning.

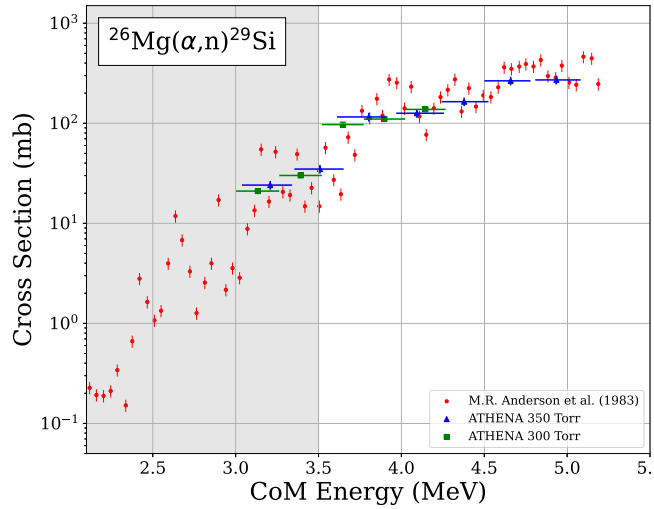

FIG. 9. Extracted total cross section for ^{26}Mg$(\alpha, n)^{29}$Si. The shaded area indicates the Gamow window for C/Ne burning.

previous data by Anderson and Van der Zwan for the ^{25}Mg reaction, and good agreement with the Anderson data for the ^{26}Mg reaction. Using the data provided by ATHENA along with the previous published data, the astrophysical reaction rates were reevaluated.

For both of these reactions, the reaction rates calculated by Angulo *et al.* above $T_9 = 2$, where $T_9 = T/10$ K, corresponding to roughly 2.5 MeV in the center-of-mass frame, were based solely on Hauser-Feshbach cross-section calculations, and not on the available experimental data [21]. Since data exist in this energy range and are in good agreement, the reaction rates are reevaluated utilizing these data. In this section, reaction rate calculations for the ^{25,26}Mg$(\alpha, n)^{28,29}$Si reactions in the temperature range above $T_9 \approx 2$ are presented. Below this temperature, which is below the energy range for the measurements made in this work, more work is needed to resolve discrepancies in the available cross section data.

Calculations of the reaction rate for the ^{25}Mg$(\alpha, n)^{28}$Si reaction in this work include data from ATHENA, Van der Zwan *et al.*, and Anderson *et al.* In the energy range below 2.0 MeV, the Anderson data are only upper limits and therefore are not used. The reaction rate was calculated using the computer code EXP2RATE [22] and is displayed with the Angulo rate in Fig. 10. A ratio of the rate in this work over the Angulo rate is shown in Fig. 11. The reaction rate for the ^{25}Mg$(\alpha, n)^{28}$Si shows an enhancement over the NACRE rate for most of the temperature range. At the peak temperature of explosive C/Ne burning ($T_9 = 2.3$), where the ^{25}Mg$(\alpha, n)^{28}$Si reaction was shown to impact ^{26}Al production, the rate of this work is slightly increased at a ratio of 1.09 over the NACRE rate. The uncertainty in the rate at this temperature is approximately 15%.

Calculations of the reaction rate for the ^{26}Mg$(\alpha, n)^{29}$Si reaction in this work include data from ATHENA and Anderson *et al.* Below 2.2 MeV, the data from Anderson are upper limits and therefore not used. The rates and corresponding ratio are shown in Figs. 10 and 11. The ratio shows enhancement across the entire temperature range. At

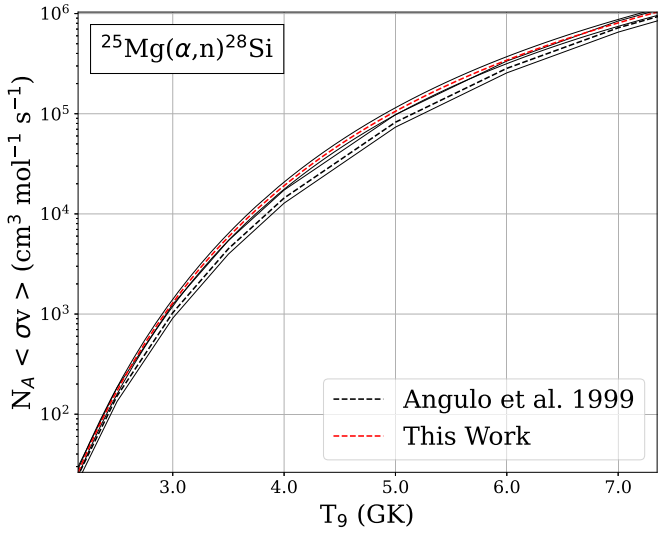

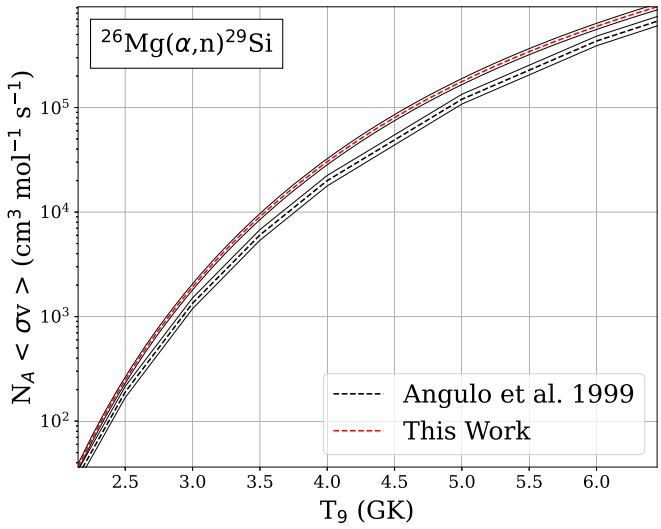

FIG. 10. Reaction rates for the ^{25,26}Mg$(\alpha, n)^{28,29}$Si reaction.

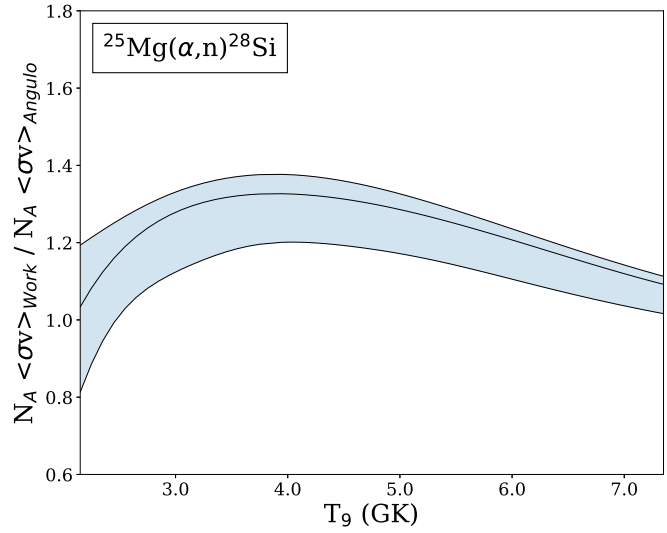

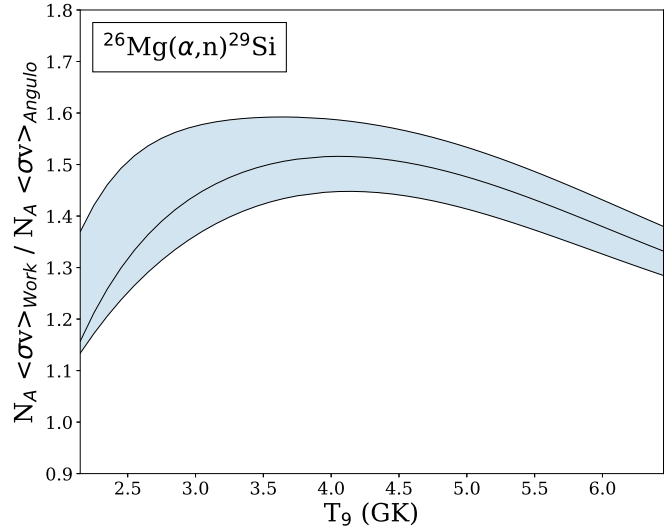

FIG. 11. Ratio of the reaction rates from this work over the work of Angulo *et al.*

the peak temperature of explosive C/Ne burning ($T_9 = 2.3$), the rate of this work is increased at a ratio of 1.24 over the NACRE rate. The uncertainty in the rate at this temperature is approximately 14%.

The analytic expression for the reaction rate as a function of temperature is given by the parametrization from [23],

$$N_A\langle\sigma v\rangle = \sum_{i=1}^{2} \exp\left[a_{i1} + \sum_{j=2}^{6} a_{ij} T^{2j/3-7/3} + a_{i7}\ln T\right], \quad (1)$$

where the reaction rate is given in cm^3/(mole s), a_{ij} are the fit parameters, and T is the temperature in units of GK. The fit parameters for both reactions are displayed in Tables III and IV.

VII. CONCLUSIONS

The observation of gamma rays from the β decay of ^{26}Al provides direct evidence of ongoing nucleosynthesis in the galaxy. Sensitivity studies have found that two reactions contributing to the uncertainty of ^{26}Al production in massive stars

TABLE III. ^{25}Mg$(\alpha, n)^{28}$Si reaction rate fit parameters.

Fit parameter	$i = 1$	$i = 2$
a_{i1}	−4.40355	3.26146
a_{i2}	−8.34444	−15.90223
a_{i3}	−6.40099	−0.11827
a_{i4}	−1.67406	4.12967
a_{i5}	4.05284	−1.47678
a_{i6}	−0.44543	0.09236
a_{i7}	2.39565	6.54141

TABLE IV. ^{26}Mg$(\alpha, n)^{29}$Si reaction rate fit parameters.

Fit parameter	$i = 1$	$i = 2$
a_{i1}	0.894420	4.121622
a_{i2}	−11.676306	−23.454746
a_{i3}	−3.794132	4.677172
a_{i4}	4.298318	3.704783
a_{i5}	−3.639849	0.688941
a_{i6}	0.323113	−0.187327
a_{i7}	13.138584	1.375834

are the ^{25}Mg$(\alpha, n)^{28}$Si and ^{26}Mg$(\alpha, n)^{29}$Si reactions. These reactions influence ^{26}Al production in stable and explosive C/Ne shell burning in massive stars. The ^{26}Mg$(\alpha, n)^{29}$Si has also been found to have a direct influence on the isotopic ratio of ^{29}Si/^{30}Si found in presolar grains formed from supernova. Models of supernova nucleosynthesis have failed to reproduce this ratio.

New measurements of the ^{25}Mg$(\alpha, n)^{28}$Si and ^{26}Mg$(\alpha, n)^{29}$Si total cross sections were made using the newly developed active-target/detector ATHENA. By measuring these reactions in ATHENA, a cross-check is provided, using an entirely different technique than the previous measurements. Through an extensive event-filtering process, (α, n) events were separated from background events and total angle-integrated and energy-integrated cross sections were extracted. The measurements provided by ATHENA are in good agreement with previous measurements in the energy range covered. With the previous cross section measurements, reaction rates have been reevaluated in the temperature region above $T_9 \approx 2$, whereas previously the rates were based solely on theoretical Hauser-Feshbach calculations.

The ^{25}Mg$(\alpha, n)^{28}$Si reaction rate calculated in this work showed a slight enhancement over the previous rate by Angulo *et al.* In explosive C/Ne burning, an enhancement in this reaction rate would imply greater destruction of seed ^{25}Mg, thus lowering overall production of ^{26}Al in massive stars. In convective C/Ne shell burning, where this reaction was found to influence ^{26}Al destruction as a neutron source, the Gamow window at $T_9 = 1.5$ is well below the measurements made in this work [2]. Regardless, more work is needed to measure the cross section at lower energies within the Gamow window for ^{26}Al production in both stable and explosive C/Ne shell burning, specifically below $E_{\text{c.m.}} = 3.00$ MeV.

The ^{26}Mg$(\alpha, n)^{29}$Si reaction rate calculated in this work also showed a slight enhancement over the previous rate by Angulo *et al.* Again, the Gamow window for convective C/Ne shell burning is well below the measurements in this work. An increase in this rate may indicate increased production of ^{29}Si in explosive C/Ne burning, which is needed for models to match isotopic ratios of ^{29}Si/^{30}Si found in the presolar grain in the work of Hoppe *et al.* [5]. Again, more work is needed to measure the cross section below $E_{\text{c.m.}} = 3.0$ MeV.

ACKNOWLEDGMENTS

This work was supported by the National Science Foundation Grant No. PHY-2310059 and by the University of Notre Dame.

[1] A. M. Laird, M. Lugaro, A. Kankainen, P. Adsley, D. W. Bardayan, H. E. Brinkman, B. Côté, C. M. Deibel, R. Diehl, F. Hammache, J. W. den Hartogh, J. José, D. Kurtulgil, C. Lederer-Woods, G. Lotay, G. Meynet, S. Palmerini, M. Pignatari, R. Reifarth, N. de Séréville *et al.*, J. Phys. G: Nucl. Part. Phys. **50**, 033002 (2023).

[2] C. Iliadis, A. Champagne, A. Chieffi, and M. Limongi, Astrophys. J. Suppl. Ser. **193**, 16 (2011).

[3] M. Limongi and A. Chieffi, Astrophys. J. **647**, 483 (2006).

[4] R. Diehl, M. Lugaro, A. Heger, A. Sieverding, X. Tang, K. A. Li, E. T. Li, C. L. Doherty, M. G. H. Krause, A. Wallner, N. Prantzos, H. E. Brinkman, J. W. den Hartogh, B. Wehmeyer, A. Y. Lopez, M. M. M. Pleintinger, P. Banerjee, and W. Wang, Pub. Astron. Soc. Aust. **38** (2021).

[5] P. Hoppe, J. Leitner, B. S. Meyer, L.-S. The, M. Lugaro, and S. Amari, Astrophys. J. **691**, L20 (2009).

[6] P. Mohr, Phys. Rev. C **97**, 064613 (2018).

[7] J. K. Bair and H. B. Willard, Phys. Rev. **128**, 299 (1962).

[8] J. Russell, W. Taylor, F. Dunnam, and H. Van Rinsvelt, Nucl. Phys. A **187**, 449 (1972).

[9] L. Van der Zwan and K. W. Geiger, Nucl. Sci. Eng. **79**, 197 (1981).

[10] M. Anderson, L. Mitchell, M. Sevior, and D. Sargood, Nucl. Phys. A **405**, 170 (1983).

[11] W. M. Howard, W. D. Arnett, D. D. Clayton, and S. E. Woosley, Astrophys. J. **175**, 201 (1972).

[12] A. Caciolli, T. Marchi, R. Depalo, S. Appannababu, N. Blasi, C. Broggini, M. Cinausero, G. Collazuol, M. Degerlier, D. Fabris, F. Gramegna, M. Leone, P. Mastinu, R. Menegazzo, G. Montagnoli, C. R. Alvarez, V. Rigato, and O. Wieland, Eur. Phys. J. A **50**, 147 (2014).

[13] O. Wieland, Diploma thesis, IFS-University of Stuttgart, 1995 (unpublished).

[14] S. Falahat, Experimental investigation of the reactions ^{25}Mg$(\alpha, n)^{28}$Si, ^{26}Mg$(\alpha, n)^{29}$Si, ^{18}O$(\alpha, n)^{21}$Ne and their impact on stellar nucleosynthesis, Ph.D. thesis, Johannes Gutenberg-Universität, 2010 (unpublished).

[15] D. Blankstein, D. Bardayan, J. Allen, C. Boomershine, L. Callahan, S. Carmichael, S. Henderson, and P. O'Malley, Nucl. Instrum. Methods Phys. Res., Sect. A **1047**, 167777 (2023).

[16] M. Skulski, T. Anderson, L. Callahan, A. Clark, A. Nelson, D. Robertson, E. Stech, and P. Collon, Nucl. Instrum. Methods Phys. Res., Sect. B **488**, 30 (2021).

[17] M. Avila, K. Rehm, S. Almaraz-Calderon, A. Ayangeakaa, C. Dickerson, C. Hoffman, C. Jiang, B. Kay, J. Lai, O. Nusair,

R. Pardo, D. Santiago-Gonzalez, R. Talwar, and C. Ugalde, Nucl. Instrum. Methods Phys. Res., Sect. A **859**, 63 (2017).

[18] J. F. Ziegler, M. Ziegler, and J. Biersack, Nucl. Instrum. Methods Phys. Res., Sect. B **268**, 1818 (2010).

[19] O. Tarasov and D. Bazin, Nucl. Instrum. Methods Phys. Res., Sect. B **376**, 185 (2016).

[20] K. Braune, R. Novotny, D. Pelte, D. Husar, and D. Schwalm, *Proceedings of the Spring Meeting of the German Physical Society* (German Physical Society, Bad Honnef, 1978), Vol. 4.

[21] C. Angulo, M. Arnould, M. Rayet, P. Descouvemont, D. Baye, C. Leclercq-Willain, A. Coc, S. Barhoumi, P. Aguer, C. Rolfs, R. Kunz, J. Hammer, A. Mayer, T. Paradellis, S. Kossionides, C. Chronidou, K. Spyrou, S. Degl'Innocenti, G. Fiorentini, B. Ricci *et al.*, Nucl. Phys. A **656**, 3 (1999).

[22] T. Rauscher, Exp2rate, https://download.nucastro.org/codes/exp2rate.f90.

[23] T. Rauscher and F.-K. Thielemann, At. Data Nucl. Data Tables **75**, 1 (2000).